Hindawi
Advances in Materials Science and Engineering
Volume 2020, Article ID 4851291, 9 pages
https://doi.org/10.1155/2020/4851291

Research Article

Effect of Clogging on the Permeability of Porous Asphalt Pavement

Yaolu Ma, Xianhua Chen, Yanfen Geng, and Xinlan Zhang

School of Transportation, Southeast University, Nanjing, Jiangsu 211189, China

Correspondence should be addressed to Xianhua Chen; chenxh@seu.edu.cn

Received 6 September 2019; Accepted 14 January 2020; Published 5 February 2020

Academic Editor: Guillaume Bernard-Granger

The purpose of this paper is to report on the drainage of porous asphalt pavement evaluation method suited for use in analyzing clogging effect. To preliminarily reveal the decrease in permeability caused by clogging of permeable asphalt pavement, an innovative device was proposed to evaluate the anisotropy of permeability influenced by clogging, and the maximum drainage capacity without surface ponding can be obtained when the supplied water was controlled. Then, finite element models for asphalt pavements with hydromechanical coupling were proposed based on porous media theory and Biot's theory. The variation in pore water pressure was simulated by considering the decrease in voids and the increase in clogging grains. The results indicate that the internally retained water should not be ignored because the semiconnected voids were filled with water rapidly at the beginning of permeability tests. To avoid surface ponding, the drainage capacity coefficient (DCC) can be used to evaluate the maximum drainage capacity (MDC) influenced by clogging. Moreover, the pore water pressure increased due to the reduction in voids and a high level of clogging. In addition, the peak value of pore water pressure is also affected by the upper-layer height of the pavement. Under the action of clogging and driving load, a reasonable thickness of the upper layer and a drainage evaluation should be considered to improve road safety.

1. Introduction

Permeable pavements have recently received great attention for improving driving safety because of their good drainage performance [1]. Porous asphalt mixtures play an essential role in permeable pavements as the material that is affected by moisture [2]. The main function of porous asphalt mixtures is to eliminate pavement flooding. The rapid removal of excess water is vital to ensure good soil and material behavior in layered pavement systems [3]. In addition, permeable pavements continue to represent an excellent form of source control for both surface runoff and pollutants [4]. A durable and sustainable drainage capability offers economic and social benefits in an environmentally friendly manner [5, 6]. During the service life of permeable pavements, there are many factors that cause the early decline in drainage, including the decrease in voids caused by clogging [7]. The clogging characteristic of the porous asphalt pavement is a common problem owing to deposition of sediments on the pavement surface, the storm water, and vehicles. It happens over time. The pavement tended to be impermeable when the pores of pavement become clogged and it performs as an ordinary dense-graded asphalt pavement, so the advantages of good performance on drainage are no longer comprehended. There is not enough literature that evaluates permeability and the effect of clogging. Therefore, the depiction of permeability evaluation influenced by clogging is a facing challenge and it is worthwhile devoting much effort to this.

Generally, the void ratio of porous asphalt pavement is more than 18% and is even as high as 23% or 25% to ensure drainage. Researches have been carried out to investigate the permeability of porous asphalt mixtures [8, 9]. Past experience has shown that a large amount of flow occurred in the horizontal direction in coarse superpave mixes with thick lifts, whereas fine mixes with thin lifts tended to have more of a vertical flow [10–12]. It is no surprise that permeability anisotropy has been the key to evaluating pavement drainage

[13]. To be precise, the water flow inside the pavement is susceptible to horizontal permeability rather than vertical permeability because the pavement is a two-dimensional surface with a thickness of 4–6 cm. Studies on the laboratory testing method for the anisotropic effect of permeability are limited, mainly because there is currently no experimental equipment or test method available to measure the permeability of porous asphalt mixtures in different directions [14]. Some researchers have proposed or optimized a number of devices that can mainly be divided into two types: varying head and constant head [15, 16]. However, it is still difficult to unify the experimental results because of the test conditions. Both the constant head and falling head laboratory methods were available to determine the permeability of the asphalt mixture. Specimens' sides were sealed by using a membrane and a confining pressure to prevent edge leakage. There was some evidence that the falling head device was the better device for testing both cores and molded cylindrical specimens [17]. However, the permeability in the two-dimensional pavement is not easy to be described. Moreover, under field conditions, the permeability process in pavement belongs to nonpressure flow when the vehicle load is neglected. The traditional approach of a constant head provides a pressure flow on the surface, and the maximum permeability can be measured, but the water supply condition is different from that in the field. This is also the reason why the laboratory results are larger than field results.

Permeable pavements are prone to clogging in the early three years [18–20]. It has been observed that the sediment contained in precipitation or runoff caused clogging and led to a reduction of 59%–75% in permeability [21]. The clogging progression rates depend on pavement characteristics, precipitation parameters, and drainage area. In addition, the clogging progression and the decrease in permeability rates in different directions are greatly affected by the pavement slope [22]. For porous asphalt mixture, specimens with a large porosity are easily clogged. Sediment particles with a size fraction of 0.15 mm−2.36 mm are used to clog the voids in specimens in laboratory tests [18]. The results of the clogging tests are insufficient because smaller particles are easily drained when the water head is higher or the water flow is faster in the specimens with large porosity. In addition, the larger particles may cause a heterogeneity clog in the surface of the specimens, which would cause variability in the measurement results. As a result, how to choose the appropriate grains to clog voids is needed to be investigated, which is beneficial for studying the effect of clogging on the permeability.

This study aims to study the anisotropy of permeability in porous asphalt mixtures and the clogging influence. Laboratory tests are performed using an innovative continuous permeability measurement that can measure the horizontal permeability capacity of specimens. Various precipitation intensities and void rates were carried out, and the water volume that drained horizontally was collected during a certain period. In addition, grains are selected as a clogging material based on investigation in the field. Indexes, including water retention, horizontal permeability, and permeability decrease influenced by clogging, are investigated to evaluate porous asphalt mixtures. Moreover, a numerical model with a hydrodynamic response is proposed based on porous media theory and Biot's theory. The vertical pore water pressure was simulated to analyze the influence of clogging on the permeability of pavement with different voids.

2. Test Material

Asphalt binder modified by styrene-butadiene-styrene (SBS) and crumb rubber was provided by Jiangsu Baoli International Investment Co., Ltd. (Wuxi, China). Properties shown in Table 1 were well enough for the porous asphalt mixture. Considering that the porous asphalt concrete with nominal maximum aggregate size less than 13 mm, namely, PAC-13, is widely used in asphalt pavement in China [23]. According to the gradation range specified in Specifications for Design of Highway Asphalt Pavement of China, specimens with a size of 300 mm × 300 mm × 5 mm were prepared by wheel rolling in the laboratory. The mixture design method used in this study is presented by the specification JTG D50 in China. The gradation curves of the asphalt mixture are shown in Figure 1. The void rate included 25%, 23%, 20%, and 18%, and the road performance test results are shown in Table 2.

3. Laboratory Modeling

3.1. Test Device. To measure the horizontal permeability, in this study, a device is optimized as shown in Figure 2. The device contains the precipitation supply part, specimen platform, and collection channel. The functions are as follows: (1) to provide controlled precipitation, (2) to distinguish the horizontal permeability from a complete rain event, and (3) to obtain the quantitative recording of permeability in the cross and longitudinal directions with consideration of the pavement slope. In this study, the supplied water volume can be controlled to simulate the operating state of the porous mixture in the field. Water volume in the collection channel is recorded during a certain period. Then, the permeability in different directions can be obtained by calculation. Therefore, the drainage capability of the porous asphalt pavement can be evaluated by obtaining the permeability in different directions.

During the test, the water supply speed should be appropriate so that no ponding occurs on the surface of the specimen. The water volume is collected, and the time of the permeation process is also recorded under normal temperature. The permeability coefficient was calculated according to the following equation:

$$n = v \cdot s^{-1} \cdot t^{-1}, \quad (1)$$

where n represents the permeability coefficient, cm/s; v is the supplied water quantity, ml; s is the cross section, cm^{-2}; and t is the time of the water flowing through the specific cross section, s.

3.2. Retention Water. The total porosity can be divided into three parts: effective porosity, semieffective porosity, and

Table 1: Properties of modified asphalt binder.

Index	Test	Requirement	Test method
Penetration at 25°C (0.1 mm)	71.3	50–80	T0604
Softening point (°C)	90.2	≥80	T0606
Ductility at 5°C (cm)	41	≥30	T0605
Kinematical viscosity at 175°C (Pa·s)	1.245	≤1.5	T0625
Elastic recovery at 25°C (%)	92	≥85	T0620
TFOT			
Mass loss (%)	0.25	≤0.6	
Residual penetration ratio at 25°C (%)	91.8	≥70	T0609
Residual ductility at 5°C (cm)	30	≥20	

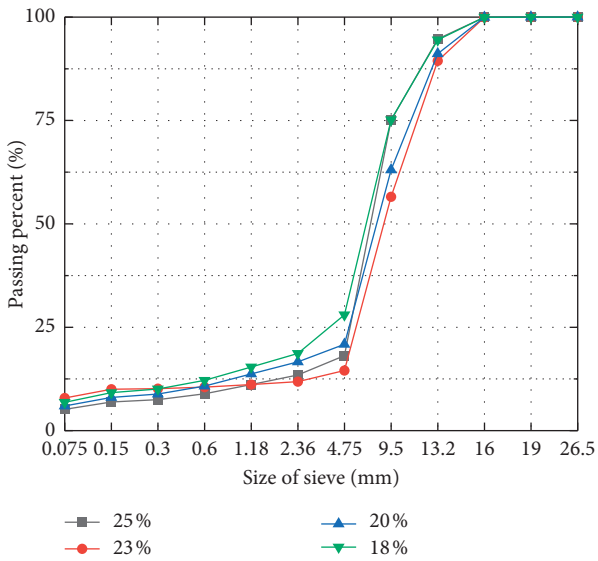

Figure 1: Gradation curves.

Table 2: Road performance of porous asphalt mixture.

Index	Tested value				Test method
Target void rate (%)	25	23	20	18	—
Real void rate (%)	26.16	21.74	19.72	17.66	T0708
Asphalt content (%)	3.50	4.20	4.20	4.50	—
Cantabro test loss (%)	19.82	13.17	7.48	4.46	T0733
Binder drainage (%)	0.05	0.5	0.04	0.18	T0732
Marshall stability (kN)	4.70	5.10	5.42	7.48	T0709
Flow value (0.1 mm)	2.51	2.68	2.82	3.48	T0709
Residual stability (%)	80	82	84	86	T0709
Dynamic stability (times/mm)	7000	6461	9333	8400	T0719

invalid porosity. The interconnected part of the pore system is defined as the effective porosity. For water, only those pores that are interconnected are important. However, the semieffective porosity, shown in Figure 3, should not be neglected because water can be stored in pores during a precipitation event. The water filling semiconnected voids is

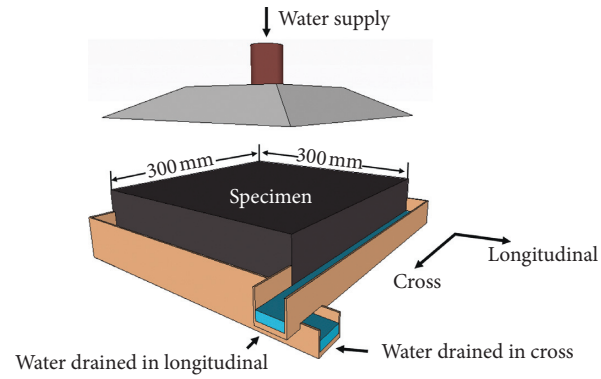

Figure 2: Measurement device.

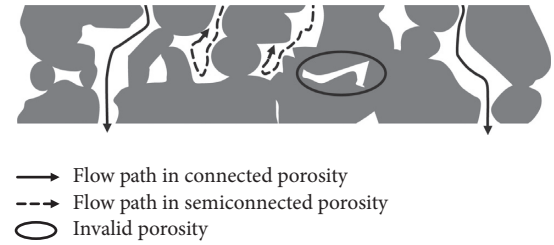

Figure 3: Porosity inside the asphalt mixture.

not easily drained by gravity, which may decrease the performance of pavement structures and materials. On the other hand, the drainage capacity can be evaluated when semiconnected voids have been confirmed.

To obtain the connected porosity of the porous asphalt mixture, the test in terms of weight was conducted. It was assumed that the semiconnected porosity was filled with water, water could not enter the invalid porosity, and water could be drained by the connected porosity. Based on the conservation of mass, the specimen mass after test increased for the reason that the semiconnected porosity was filled with water. Then total mass included the mass of dry specimen and water in semiconnected porosity. The semiconnected porosity volume could be depicted by

$$v_1 = (m_1 - m_2) \times \rho^{-1}, \quad (2)$$

where v_1 is the semiconnected porosity volume, m^3; m_1 is the dry mass of the specimen before immersion in water, g; m_2 is the mass of the specimen when the water in the connected porosity was drained after immersion; and ρ is the water density, g/cm^3.

Once the semiconnected porosity was obtained according to the weight test, the connected porosity can be presented as shown in Table 3. It should be noted that the test results of the semiconnected ratio here may be slightly larger than the results from the test method of complete immersion in water. The results here demonstrated that the water retention after drainage is significant for investigating the pavement dry-wet condition after a precipitation event. It can be concluded that the retention water decreased after the rutting test. However, the decline increases as the void

Table 3: Average value of retained water before and after the rutting test.

Void ratio (%)	Before rutting test (ml)	After rutting test (ml)
25	232	228
23	220	206
20	198	161
18	136	90

ratio decreases. This result can be explained by the fact that a higher void ratio has a better structural frame due to the gradation. The size of grains may influence the void distribution inside the specimen. Compared with specimens with low void ratio, specimens with high void ratio may store more water and have better stability when suitable gradations are designed. As a result, reasonable adjustment of the gradation design for pavement drainage can effectively reduce the retained water, thereby improving the stability and durability of the pavement.

3.3. Clogging. Similar to a previous article [18], clogging materials are the sediments that were collected after the rainfall. The location of the test site is on Shiyang Road in Nanjing, and the upper layer of the nonmotor vehicle lane is porous asphalt pavement, which facilitates collecting the sediment from precipitation runoff. In this study, the clogging material was composed of fine and coarse sizes, and the mixture of particle sizes ranged from 0.15 mm to 2.36 mm (Table 4). The initial precipitation intensity was assumed to be 80.73 ml/min after measurement, and then the drained water was collected from the collection channel.

To avoid surface ponding, the general behavior of a porous pavement system is that, up to a certain rainfall depth, the system fills and does not have any runoff. The maximum drainage capacity (MDC) of specimens can be obtained by controlling the supplied water under these conditions (Figure 4). The MDC is defined as the supplied water discharge for the specimens with a surface size of 30 cm * 30 cm in the laboratory. So the value of MDC is equal to the precipitation intensity for specimens with different void ratio. The drainage capacity coefficient (DCC) is defined as the ratio of the water discharge and drainage time. The results in Table 5 are the average of three specimens for five measurement times.

The results showed that the variation of horizontal permeability is much more obvious influenced by void ratio. The various void ratio causes the greatest change in the permeability in the different directions tested. Differences are likely due to the connected voids declining when the flow seepage becomes greater in the vertical dimension. These results also clearly indicated that the clogging grains actually reduced the permeability of the porous specimens. The surface inundation occurred (Figure 5) if the supplied water exceeded the MDC. The MDC exhibited a decline when the clogging increased, which indicates that the increase in clogging has made drainage decline in a short time. The difference between the two directions in horizontal is caused by the washing from water flow in the internal direction of the specimen. LV is generally larger than CV due to the small slope. It should be noted that the reduction in specimens with various void ratios seemed quite different; one reason

Table 4: Clogging mixtures.

Particle size (mm)	Sieve pass ratio (%)
Above 2.36	100
1.18	73
0.6	41
0.3	17
0.15	0

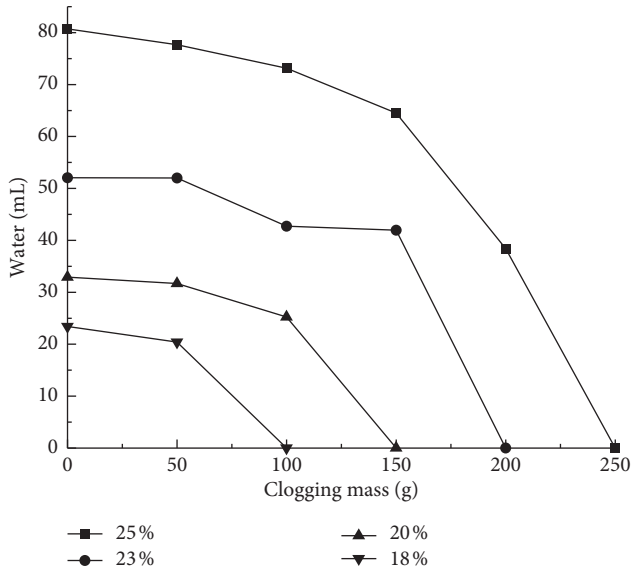

Figure 4: MDC influenced by clogging.

may be that the specimens have different gradations and uneven clogging distributions. Another reason may be that the connected voids in the vertical direction are prone to be clogged, and then the voids in the horizontal direction are clogged. A certain number of connected voids are changed into semiconnected voids (Figure 6).

3.4. Hydromechanical Coupling. Referred to Biot's theory, the basis of dynamic response process includes principle of effective stress, law of conservation of mass, Darcy's law, momentum conservation, and constitutive equation [24]. The dynamic balance equation is as follows:

$$G\nabla^2 u + \frac{G}{1-2\nu}\nabla \operatorname{div} u = \nabla p + (1-n)\rho_s \frac{\partial v_s}{\partial t} + n\rho_f \frac{\partial v_f}{\partial t}, \quad (3)$$

where u is displacement vector, v_s is solid velocity vector, v_f is fluid velocity vector, G is shear modulus of medium, ν is Poisson's ratio, p is pore pressure, n is porosity of porous medium, ρ_s is medium density, and ρ_f is fluid density.

The permeability of porous media is used to depict the fluid flow in porous media in this model. According to Darcy's law, the relationship between the liquid flow velocity in porous media and the external pressure can be depicted by the momentum equation of pore fluid:

$$v = -\frac{k}{\mu}\frac{\partial p}{\partial x}, \quad (4)$$

Table 5: Drainage decline of various void rates.

Void rate (%)	CM (g)	LV (ml/s)	CV (ml/s)	MDC (ml/s)	DT (s)	DCC
25	0	45.45	39.71	80.73	14.63	5.52
	50	36.57	34.65	77.66	18.06	4.30
	100	35.62	30.44	73.14	20.40	3.59
	150	32.60	26.97	64.51	18.17	3.55
	200	15.6	21.42	38.40	13.40	2.87
23	0	30.64	26.02	55.04	16.71	3.29
	50	25.24	22.56	51.99	19.86	2.62
	100	22.86	20.28	42.72	24.35	1.75
	150	20.15	20.84	41.94	25.61	1.64
20	0	21.02	13.39	32.9	15.75	2.09
	50	18.70	13.89	31.67	18.52	1.71
	100	16.70	6.76	25.24	16.13	1.56
18	0	12.37	10.27	23.40	13.81	1.69
	50	11.74	8.39	20.39	23.27	0.88

CM: clogging mass. LV: longitudinal velocity. CV: cross velocity. MDC: maximum drainage capacity. DT: drainage Time. DCC: drainage capacity coefficient.

(a) (b)

Figure 5: MDC measurement ((a) surface drainage; (b) surface inundation).

where k is the permeability coefficient in porous media and μ is the viscosity coefficient.

A finite element method analysis of the porous pavement was conducted to explore the pore pressure and tensile stress distribution. All material properties were assumed to be elastic. The pavement model was composed of the structure layer, upper layer, midsurface, lower layer, base, subbase, and embankment. The upper layer is made of porous asphalt pavement. In this model, the bottom boundary of the model was in full constraint, the boundary was constrained in the normal direction, and the upper boundary was free. Because the upper layer of this model was permeable pavement, the initial pore water pressure of each layer was assumed to be 0. In the porous media of the saturated bitumen, the solid phase was a skeleton structure of the asphalt mixture. Referred to [25], the material parameters of the pavement structure are listed in Table 6.

AC-20: asphalt concrete (maximum nominal size is 20 mm). CTB: cement stabilized macadam.

In this paper, the pressure was assumed to be evenly distributed on the pavement surface. The vehicle was simplified as a uniform circular load, and the internal pressure of the tire was regarded as acting on the pavement. In the specifications of asphalt pavement design in China, $F_{\max} = 0.7$ MPa. The loading curve F versus time is shown in Figure 7 and is calculated by the following equations. The load position was located at the center position.

$$F = \sigma \times S,$$

$$\sigma = P_{\max} \cdot \sin\left(\frac{\pi}{t} T\right), \quad 0 \le T \le T_1, \tag{5}$$

$$\sigma = 0, \quad T > T_1,$$

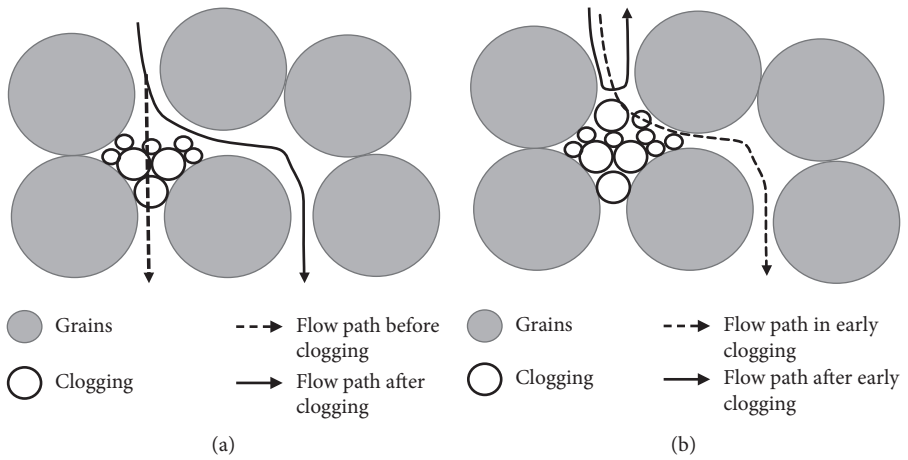

Figure 6: The internal clogging.

Table 6: Material parameters of the model structure.

Structure layer	Elastic modulus (MPa)	Density (kg/m^3)	Poisson's ratio	Permeability coefficient (10^{-4} cm/s)
Upper layer (PAC-13)	800	2100	0.30	7.8–30.3
Midsurface (AC-20)	1400	2400	0.35	0.1
Lower layer (AC-20)	1400	2400	0.35	0.1
Base (CTB)	1600	2100	0.20	1
Subbase (lime-ash soil)	600	1900	0.30	0.01
Embankment (soil)	50	1900	0.40	0.01

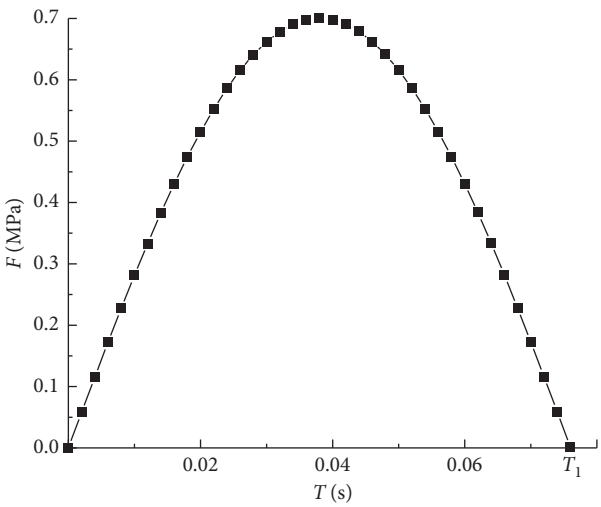

Figure 7: Loading curve of wheel load.

where F is the load on the wheel, kN; σ is the tire contact pressure, kPa; S is the equivalent area of the load acting on the pavement; and T_1 is the acting time of a single vehicle. When the velocity is 60 km/h, the equivalent T_1 is approximately 0.076 s.

Based on the basic assumption of a layered elastic system for pavement structure and elastic dynamics theory, the control equations of the dynamic response of pavement structure are as follows:

$$[\mathbf{M}]\{\ddot{u}\} + [\mathbf{C}]\{\dot{u}\} + [\mathbf{K}]\{u\} = \{F(t)\}, \tag{6}$$

where $[\mathbf{M}]$ is the mass matrix, $\{\ddot{u}\}$ is the node acceleration, $[\mathbf{C}]$ is the damping matrix, $\{\dot{u}\}$ is the node speed, $[\mathbf{K}]$ is the stiffness matrix, $\{u\}$ is the node displacement vector, and $\{F(t)\}$ is the load vector acting on the node.

According to the article [26], the Rayleigh damping assumption is usually adopted to express the damping matrix as a linear combination of the mass matrix and the stiffness matrix. It can be presented as

$$\{\mathbf{C}\} = \alpha\{\mathbf{M}\} + \beta\{\mathbf{K}\}, \tag{7}$$

where α and β are the damping coefficient related to the natural frequency and the damping ratio of the structure.

In (7),

$$\alpha = \frac{2\omega_1\omega_2\left(\omega_2\xi_1 - \omega_1\xi_2\right)}{\omega_2^2 - \omega_1^2},$$
$$\beta = \frac{2\left(\omega_2\xi_2 - \omega_1\xi_2\right)}{\omega_2^2 - \omega_1^2}, \tag{8}$$

where ω_2 and ω_2 are the pavement natural frequency and ξ_1 and ξ_2 are the damping ratio.

Figures 8 and 9 clearly indicated that there was a rapid increase in the pore water pressure and a rapid dissipation that followed. The positive and negative pressures increased noticeably at both depths (3 cm and 6 cm) in the upper layer of the pavement when the clogging grains were added. The value of the pore water pressure in the middle location (3 cm) was less than that in the bottom location (6 cm). The internal pore water pressure was larger than that at the surface. For example, once the clogging grain mass increased from 50 g to

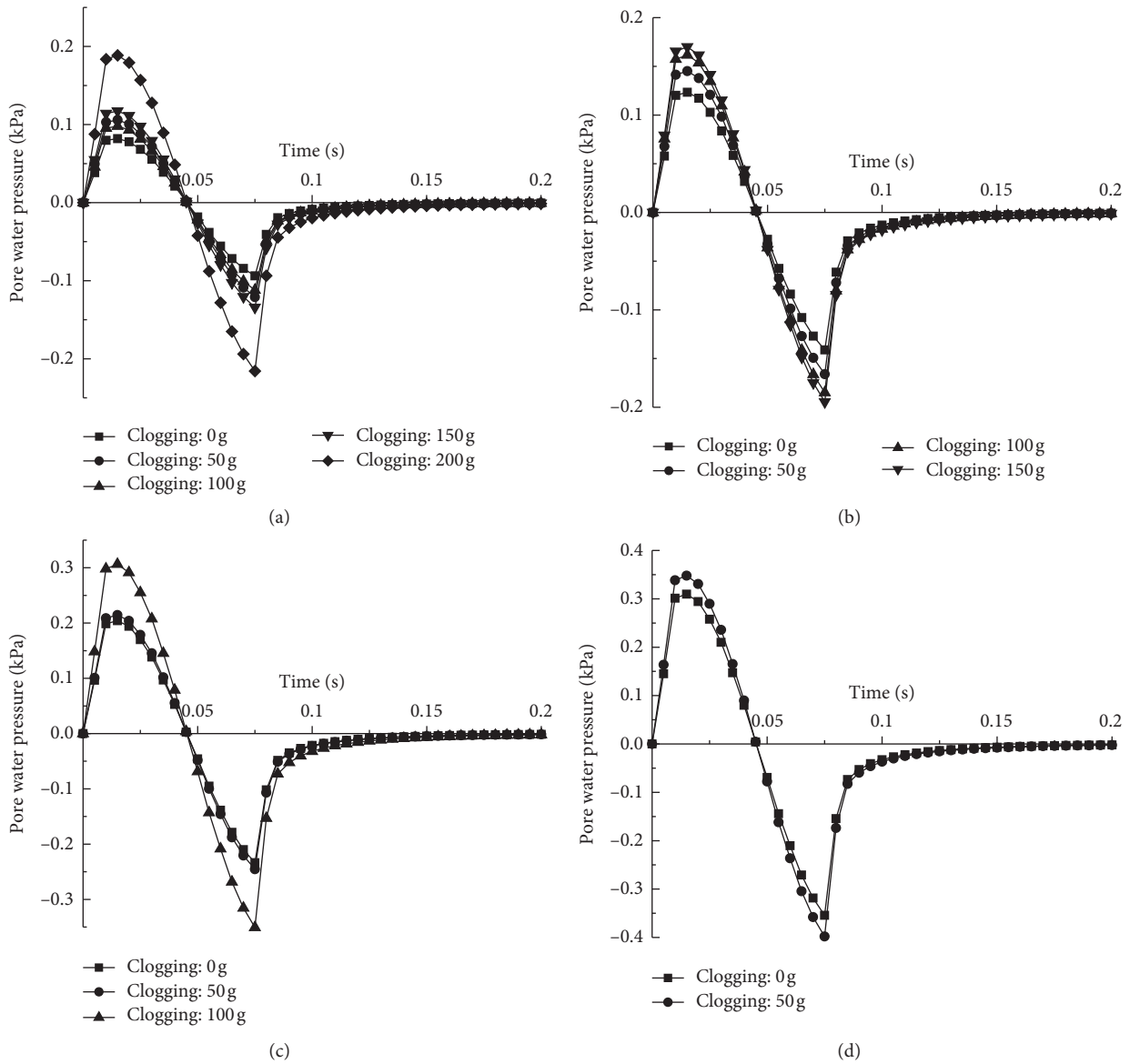

Figure 8: Pore water pressure at a depth of 3 cm ((a) void rate is 25%; (b) void rate is 23%; (c) void rate is 20%; (d) void rate is 18%).

200 g in the specimen with a void ratio of 25%, the maximum positive pore water pressure increased from 0.08 kPa to 0.19 kPa at a depth of 3 cm, while the negative pore water pressure peak changed from −0.09 kPa to −0.22 kPa. However, in the bottom location (6 cm), the maximum positive pore water pressure increased from 0.1 kPa to 0.23 kPa at a depth of 3 cm, while the negative pore water pressure peak changed from −0.12 kPa to −0.26 kPa.

As the void ratio decreased to 18%, the pore water pressure increased substantially because the pores became less easily filled with water. That is, the pavement surface might be subject to a greater external pressure when the pores were clogged. Although the influence of pore water flow on the asphalt mixture might be disregarded, a certain clogging degree was shown to be harmful to the asphalt mixture considering the pore water pressure. Because more surface area was exposed to air and water compared to that of dense-graded asphalt pavement, repeated suction could decrease the cohesion between the asphalt and aggregate. Cracks or other imperfections were more likely to be induced in the pavement, consequently reducing the strength of the material and the service life of the pavement.

4. Conclusions

To study the retention of water and the reduction in permeability of porous drainage pavement influenced by clogging, an innovative permeability measurement was proposed to evaluate the permeability anisotropy. Laboratory tests were performed, and the maximum drainage discharge (MDD) and maximum drainage capacity (MDC) should be taken into account to demonstrate the permeability decrease. Moreover, the finite element model for porous pavement with hydrodynamic response was applied based on porous media theory and Biot's theory. The variation in pore water pressure

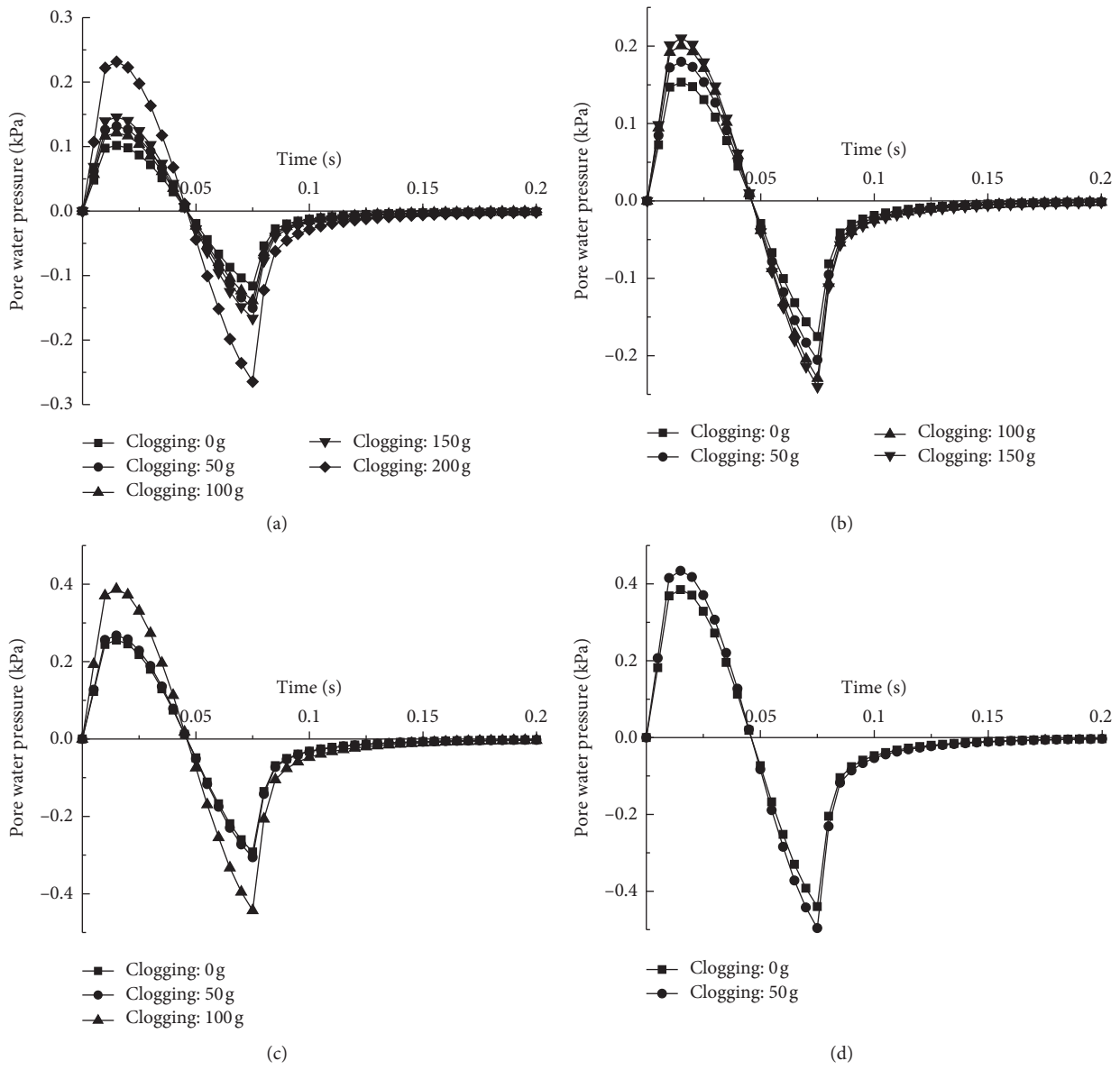

Figure 9: Pore water pressure at a depth of 6 cm ((a) void rate is 25%; (b) void rate is 23%; (c) void rate is 20%; (d) void rate is 18%).

influenced by clogging was obtained at a certain speed using the numerical model. The following conclusions are drawn:

The drainage capacity of permeable pavements is greatly decreased once the pores become clogged. The specimen can hardly drain when the clogging increases to a certain degree. Improving the water diffusion horizontally to maintain better drainage performance and avoid clogging can have a positive influence on driving safety.

Water may be retained because of voids in the pavement, and the influence of the initial water content should be taken into account in confirming the drainage capacity. The drainage capacity of porous pavement can be reflected by the anisotropy of the permeability. This anisotropy can be measured in the laboratory, and we have demonstrated the maximum drainage capacity influenced by clogging.

Porous asphalt pavement has better performance in drainage when used as the upper layer. Because of hydromechanical coupling, the pore water pressure of the permeable asphalt pavement fluctuates periodically with the fluctuation in the external load. To decrease the pore water pressure caused by repeated suction from the wheel load, an acceptable thickness should be confirmed by the consideration of drainage capacity and pavement service performance.

Data Availability

All data, models, or codes generated or used during the study are available from the corresponding author upon request.

Conflicts of Interest

The authors declare no conflicts of interest.

Acknowledgments

This research was funded by the Postgraduate Research & Practice Innovation Program of Jiangsu Province (no. KYCX18_0138) and National Natural Science Foundation of China (NSFC) (Grant nos. 51979040 and 51778136).

References

[1] T. H. Nguyen, J. Ahn, J. Lee, and J.-H. Kim, "Dynamic modulus of porous asphalt and the effect of moisture conditioning," *Materials*, vol. 12, no. 8, p. 1230, 2019.

[2] C. F. Yong, D. T. Mccarthy, and A. Deletic, "Predicting physical clogging of porous and permeable pavements," *Journal of Hydrology*, vol. 481, pp. 48–55, 2013.

[3] J.-P. Bilodeau, G. Doré, and C. Savoie, "Laboratory evaluation of flexible pavement structures containing geocomposite drainage layers using light weight deflectometer," *Geotextiles and Geomembranes*, vol. 43, no. 2, pp. 162–170, 2015.

[4] D. M. William and B. K. Nigel, "Characterization of undrained porous pavement systems using a broken-line model," *Journal of Hydrologic Engineering*, vol. 20, no. 2, Article ID 04014043, 2015.

[5] Y. Chen, G. Tebaldi, R. Roque, G. Lopp, and Y. Su, "Effects of interface condition characteristics on open-graded friction course top-down cracking performance," *Road Materials and Pavement Design*, vol. 13, no. sup1, pp. 56–75, 2012.

[6] H. Wang, C. Wang, Z. You, X. Yang, and Z. Huang, "Characterising the asphalt concrete fracture performance from X-ray CT Imaging and finite element modelling," *International Journal of Pavement Engineering*, vol. 19, no. 3, pp. 307–318, 2018.

[7] M. L. Pattanaik, R. Choudhary, and B. Kumar, "Clogging evaluation of open graded friction course mixes with EAF steel slag and modified binders," *Construction and Building Materials*, vol. 159, pp. 220–233, 2018.

[8] M. Awadalla, A. O. Abd El Halim, Y. Hassan, I. Bashir, and F. Pinder, "Field and laboratory permeability of asphalt concrete pavements," *Canadian Journal of Civil Engineering*, vol. 44, no. 4, pp. 233–243, 2017.

[9] M. O. Hamzah, M. R. M. Hasan, and M. V. D. Ven, "Permeability loss in porous asphalt due to binder creep," *Construction And Building Materials*, vol. 30, pp. 10–15, 2012.

[10] H. El-Hassan and P. Kianmehr, "Pervious concrete pavement incorporating GGBS to alleviate pavement runoff and improve urban sustainability," *Road Materials and Pavement Design*, vol. 19, no. 1, pp. 167–181, 2018.

[11] W. Jiang, A. Sha, J. Xiao, and Z. Wang, "Microscopic void features and influence of porous asphalt concrete," *Journal of Tongji University*, vol. 43, no. 1, pp. 67–74, 2015, in Chinese.

[12] S. Takahashi, "Comprehensive study on the porous asphalt effects on expressways in Japan: based on field data analysis in the last decade," *Road Materials and Pavement Design*, vol. 14, no. 2, pp. 239–255, 2013.

[13] L. Chen, "Study voids distribution of porous asphalt mixture based on industrial CT," *Highway Engineering*, vol. 41, no. 1, pp. 202–215, 2016, in Chinese.

[14] J. Chen, H. Wang, and H. Zhu, "Investigation of permeability of open graded asphalt mixture considering effects of anisotropy and two-dimensional flow," *Construction and Building Materials*, vol. 145, pp. 318–325, 2017.

[15] J. Zhang, X. Cui, L. Li, and D. Huang, "Sediment transport and pore clogging of a porous pavement under surface runoff," *Road Materials and Pavement Design*, vol. 18, no. S3, pp. 240–248, 2017.

[16] L. Cui and S. Bhattacharya, "Choice of aggregates for permeable pavements based on laboratory tests and DEM simulations," *International Journal of Pavement Engineering*, vol. 18, no. 2, pp. 162–170, 2017.

[17] J. Chen, X. Yin, H. Wang, and Y. Ding, "Evaluation of durability and functional performance of porous polyurethane mixture in porous pavement," *Journal of Cleaner Production*, vol. 188, pp. 12–19, 2018.

[18] X. Cui, J. Zhang, D. Huang, W. Tang, L. Wang, and F. Hou, "Experimental simulation of rapid clogging process of pervious concrete pavement caused by storm water runoff," *International Journal of Pavement Engineering*, vol. 20, no. 1, pp. 24–32, 2019.

[19] J. Chen, Y. Kong, X. Huang, Y. Xu, and L. Wang, "Laboratory evaluation of the effect of longitudinal rutting on transversal permeability in porous asphalt pavement," *Journal of Southeast University (Natural Science Education)*, vol. 46, no. 3, pp. 584–588, 2016, in Chinese.

[20] R. H. Jorge, C. F. Daniel, H. F. B. Andrés, and V. Z. Ángel, "Characterization of infiltration capacity of permeable pavements with porous asphalt surface using cantabrian fixed infiltrometer," *Journal of Hydrological Engineering*, vol. 17, no. 5, pp. 597–603, 2012.

[21] D. Pezzaniti, S. Beecham, and J. Kandasamy, "Influence of clogging on the effective life of permeable pavements," *Proceedings of the Institution of Civil Engineers—Water Management*, vol. 162, no. 3, pp. 211–220, 2009.

[22] H.-C. Dan, L.-H. He, L.-H. Zhao, and J.-Q. Chen, "Coupled hydro-mechanical response of saturated asphalt pavement under moving traffic load," *International Journal of Pavement Engineering*, vol. 16, no. 2, pp. 125–143, 2015.

[23] H. Wang and M. Zhou, "Drain ability and anti-clogging ability of porous asphalt mixture," *Journal of Building Materials*, vol. 19, no. 2, pp. 413–416, 2016, in Chinese.

[24] R. Ren, W. Qi, and M. Ling, "Analysis on dynamic response of saturated asphalt pavement under moving vehicle loads by 3D finite element method," *Journal of Highway and Transportation Research and Development*, vol. 28, no. 9, pp. 11–16, 2011.

[25] Z. Dong, L. Cao, and Y. Tan, "Time history analysis of dynamic response for saturated asphalt pavement," *Journal of Wuhan University of Technology*, vol. 33, no. 6, pp. 1033–1036, 2009, in Chinese.

[26] W. Hou and X. Zhao, "Response analysis of saturated asphalt pavement under action of moving load," *Highway Engineering*, vol. 21, pp. 12–15, 2012, in Chinese.